Oxid Met (2017) 87:321–332
DOI 10.1007/s11085-016-9703-3

ORIGINAL PAPER

Properties of Alumina/Chromia Scales in N_2-Containing Low Oxygen Activity Environment Investigated by Experiment and Theory

Christine Geers[1] · Vedad Babic[1] · Nooshin Mortazavi[2] · Mats Halvarsson[2] · Bo Jönsson[3] · Lars-Gunnar Johansson[1] · Itai Panas[1] · Jan-Erik Svensson[1]

Received: 21 December 2016 / Published online: 11 January 2017

Abstract The FeCrAl alloy Kanthal APMT^{TM} was exposed to N_2–5%H_2 at 900 °C. Trace oxygen in the gases supplied an oxygen activity which was sufficient to render alumina and chromia thermodynamically stable. The exposures revealed that the oxide scale was penetrated by nitrogen exclusively at chromia domains. Microscopic analyses of the oxide scale did not reveal micro-cracks that could serve as points-of-entry for nitrogen. Instead it is suggested that nitrogen is transported through a dense chromia layer. Density functional theory was employed to investigate decisive nitrogen surface chemistry and transport properties in chromia and alumina. The study was used to validate that the complex redox chemistry of Cr^{3+} as opposed to Al^{3+} is a sufficient discriminating factor between alumina and chromia, facilitating N_2 dissociation and mobility of N in chromia.

Keywords Nitridation · Alumina · Chromia · Transport properties of the oxide · Metastable phases

Introduction

FeCrAl alloys such as Kanthal APMT^{TM} provide excellent oxidation resistance at high temperatures due to the formation of slow-growing and adherent alumina scales [1, 2]. Thus, alumina scale growth prohibits the oxidation of other alloying elements such as iron and chromium and the Al_2O_3 scale protects the alloy from nitridation and carburization [3]. Here, the high thermodynamic stability of alumina

✉ Christine Geers
geersc@chalmers.se

[1] Department of Energy and Materials, Chalmers University of Technology, Göteborg, Sweden

[2] Department of Physics, Chalmers University of Technology, Göteborg, Sweden

[3] Sandvik Heating Technology AB, Hallstahammar, Sweden

relative to AlN [4] is emphasized, making Al_2O_3-forming alloys useful also in low oxygen activity nitriding environments. However, internal nitridation is an important mode of corrosion for Al_2O_3-forming alloys in environments where low oxygen activity (low dew point) is combined with a high availability of nitrogen-containing species [5]. For example, FeCrAl's have been successful in some alloy heat treatment applications [6] but were reported to suffer nitridation in very dry $N_2 + H_2$ environments [7]. Alloy nitridation dramatically decreases the aluminium activity in the alloy, causes embrittlement and destroys the integrity of the protective oxide scale. It is often considered that a continuous external Al_2O_3 scale is an effective barrier to nitrogen uptake by the alloy [7]. There are two main candidate processes whereby the Al_2O_3 scale may be short-circuited to cause nitridation. One employs cracks through the scale, allowing direct access of molecular N_2 to the metal. The second process involves ionic transport of nitrogen across the scale, through the oxide lattice or along grain boundaries. However, adopting a Wagnerian perspective, electronic conduction through the oxide scale is required in the latter case. This is satisfied by chromia, which has been reported to be present in Al_2O_3 scales in some cases [8]. In this work, the FeCrAl alloy Kanthal APMT^{TM} was exposed to a mixture of 95% N_2 and 5% H_2 at 900 °C, simulating a type of heat treatment environment encountered in steel production and sintering. The water vapour content was kept very low, in the order of 50 ppm, in order to provoke alloy nitridation. Microscopic investigation gave ample proof of alloy nitridation and showed that nitridation was associated with the appearance of chromia domains embedded in the Al_2O_3 scale. This suggested that the chromia domains were the points-of-entry for nitrogen into the alloy. The chromia domains may have formed at chromium carbides [9] or reactive element particles present at the surface prior to exposure. Hence, it was decided to use 1st principles modelling to investigate the ability of chromia to constitute a channel for nitrogen ion transport, short-circuiting the Al_2O_3 scale. Thus, the consequences exposing chromia to dual, potentially reducing, conditions are analysed. The chromia/gas interface is considered to experience a low oxygen activity, while at the chromia/alloy interface, chromia is reduced by Al in the alloy. Sufficient conditions for oxidation-driven nitridation are formulated comprising the following: (1) coordinatively unsaturated Cr sites in the chromia surface, and (2) formation of transient chromium oxy-nitrides as driven by the oxidation of aluminium by chromia. The corrosion morphology and corrosion products resulting from alloy nitridation are described and a mechanism for nitrogen penetration through the scale is formulated. A comprehensive understanding emerges by employing microscopy, thermodynamics and 1st principles modelling utilizing density functional theory (DFT).

Experimental and Theoretical Approaches

Exposure and Microscopy

The creep-resistant Al_2O_3-forming alloy Kanthal APMT^{TM} was exposed to nitriding conditions (N_2–5%H_2) at 900 °C. Trace amounts of O_2 (about 15 ppm) were

measured in the nitrogen gas via a zirconia oxygen sensor at 700 °C. Equilibrating this oxygen with hydrogen at 900 °C results into a complete conversion to steam and an oxygen activity of 10^{-23} (calculated by Factsage). The Cr_2O_3/Cr equilibrium corresponds to an oxygen activity of 10^{-25}. The nominal composition of the Al_2O_3-forming alloy investigated (Kanthal APMT^{TM}) is in Table 1. The alloy has a comparably large reservoir of aluminium (5 wt%) and is used in low oxygen activity applications. It contains minor additions of reactive elements which are known to be beneficial for the adherence of the Al_2O_3 scale and that also improve creep performance [10]. In high oxygen activity conditions, the recommended maximum operation temperature is 1250 °C.

The sample material was cut into 15 × 15 × 2 mm^3 coupons which were ground and then polished using 1-μm diamond paste. After thorough rinsing in water, ethanol and acetone assisted by ultrasound, the samples were mounted on an alumina sample holder and placed in a horizontal furnace tube. The experiment was started by purging the furnace tube with the N_2+5%H_2 gas mixture for at least 8 h to expel traces of air. After rapid heating to target temperature in 30 min, the samples were kept at 900 °C for 168 h and cooled down slowly within 5 h in the furnace afterwards. The gas flow was 100 ml/min corresponding to a net average gas flow speed of 6.3 cm/min in the tube. After exposure, the samples were subjected to several analyses starting with the determination of mass gain, surface scanning electron microscopy, backscatter electron (SEM/BSE) studies followed by focused ion beam (FIB), transmission electron microscopy (TEM) and energy-dispersive X-ray spectroscopy (EDS) when indicated. Cross sections were performed either manually via epoxy embedding, cutting and polishing or via the broad ion beam technique. In all, 32 individual samples were subjected to the nitriding gas at 900 °C and investigated after exposure to generate a good reproducibility of the here described corrosion phenomenon.

Computational Method and Details

DFT calculations employed the CASTEP code [12] within the Materials Studio 6.1 suite [13]. The Purdue–Burke–Ernzerhof functional within the generalized gradient approximation was used with a 500.0 eV plane-wave cut-off energy in conjunction with on-the-fly computed pseudopotentials. Convergence criteria for the geometry optimization calculations included 10^{-3} Å (displacement) and 10^{-5} eV/atom

Table 1 Chemical composition of alloy Kanthal APMT^{TM}

Wt%	C	Si	Mn	Mo	Cr	Al	Fe	Other[a]
Nominal				3.0	21.0	5.0	Balance	RE: Y 0.1, Hf 0.1, Zr 0.05
Min.	–	–	–		20.5			
Max.	0.08	0.7	0.4		23.5	–		

[a] Typical composition [11]

(energy). A Monkhorst–Pack k-point grid with 0.04 $Å^{-1}$ k-point separation was employed [14]. Spin-polarized calculations were performed throughout.

Validation of Method

The usefulness of the employed DFT strategy relies on it describing sufficiently well the thermodynamic drives causing the nitrogen pick-up. In order to validate this claim, relative stabilities of the Al_2O_3 and Cr_2O_3 couple, as well as those of AlN, Cr_2N, and CrN [15], were compared to experiment in the following manner:

$$Cr_2O_3(s) + 2Al(s) \rightarrow Al_2O_3(s) + 2Cr(s) \tag{1}$$

$$\Delta H_{exp} = -535 \text{ kJ/mol}; \quad \Delta H_{DFT} = -495 \text{ kJ/mol}$$

and also

$$CrN(s) + Al(s) \rightarrow AlN(s) + Cr(s) \tag{2}$$

$$\Delta H_{exp} = -201 \text{ kJ/mol}; \quad \Delta H_{DFT} = -191 \text{ kJ/mol} ,$$

where

$$\Delta H_{DFT} = \sum_{p=\text{prod}} E_{tot}[p] - \sum_{r=\text{react}} E_{tot}[r]. \tag{3}$$

Models

Two sets of calculations were performed. To address bulk transformations, straightforward calculations of unit cells of the bulk material under consideration were employed. Chemisorption of N on chromia and alumina utilized a stoichiometric periodic slab model. Cr(III)/Al(III) ion-terminated (001) surface of M_2O_3 (corundum), offering coordinatively unsaturated sites (CUS), was employed to describe the reduced gas–oxide interface and can be interpreted in terms of surface and, to some extent, grain boundary processes. This slab will in the following be denoted as $[-;-]M_{12}O_{18}(\text{slab})$ pointing to the presence of two coordinatively unsaturated metal ions on the slab surface, each exhibiting one vacant site. In this case, both sites are unoccupied, while $[N;-]M_{12}O_{18}(\text{slab})$ has one of the two sites coordinated by nitrogen. This notation allows for a convenient way to consider surface coverage.

Consider the general reaction

$$M_iN(s) + [-;A](M_i)_{12}O_{18}(\text{slab}) \rightarrow M_i(s) + [N;A](M_i)_{12}O_{18}(\text{slab}), \tag{4}$$

where $M_{i=1,2}$ = Cr, Al and [A] denotes if either (N), (O) or any (–) species occupies the CUS. The reaction enthalpy is denoted $\Delta H_M^{N;A}$ and is calculated according to (3). In the case when the experimental enthalpy of formation of MN(s) is used to shift the calculated enthalpy to arrive at the sought surface nitridation enthalpy, reaction 4 becomes

$$\frac{1}{2}N_2 + [-;A](M_i)_{12}O_{18}(\text{slab}) \rightarrow [N;A](M_i)_{12}O_{18}(\text{slab}). \quad (5)$$

And the reaction enthalpy, which is now denoted with a tilde, becomes

$$\Delta\tilde{H}_M^{N;A} = \Delta H_M^{N;A} - \Delta H_{Exp}[MN(s)]. \quad (6)$$

Analogously, for

$$N_2 + [-;-](M_i)_{12}O_{18}(\text{slab}) \rightarrow [N;N](M_i)_{12}O_{18}(\text{slab}) \quad (7)$$

we compute the reaction energy for

$$2M_iN(s) + [-;-](M_i)_{12}O_{18}(\text{slab}) \rightarrow 2M_i(s) + [N;N](M_i)_{12}O_{18}(\text{slab}) \quad (8)$$

from 1st principles and take the nitridation enthalpy from experiment to arrive at

$$\Delta\tilde{H}_M^{N;N} = \Delta H_M^{N;N} - 2\Delta H_{Exp}[MN(s)]. \quad (9)$$

Results and Discussion

The present study shows that alloy nitridation occurs in the absence of observable cracks in the oxide scale. Indeed, identification of signatures of this failure constitutes a central part of this work (see below). Hence, this paper is directed towards understanding the sequence of events that cause internal nitridation of FeCrAl steels covered by a continuous crack-free oxide scale. Owing to the localized nature of nitridation, systematic corrosion experiments in conjunction with careful microscopy is required. A combination of well-defined experiments, careful post-analysis and complementary 1st principles modelling is employed. In what follows, the characteristic microstructural signatures of internal nitridation are first presented. Based on these observations and thermodynamic considerations, a viable time evolution for the nitridation process is arrived at. A working hypothesis is subsequently formulated for how the crack-free oxide scale becomes short-circuited towards nitrogen penetration. Finally, emerging central claims of the working hypothesis, regarding thermodynamic drivers as well as the viability of transient nitrogen species, are validated by 1st principle modelling.

Microscopy of Alloy Nitridation

Figure 1 shows SEM images of an APMT^{TM} sample after 168 h N_2–5%H_2 exposure at 900 °C. Figure 1a shows a top view image at low magnification. The surface features show preferential alignment, presumably along the rolling direction. In addition to an uniform grey alumina layer (Fig. 1a, i) covering about 99% of the surface, two typical features of interest can be identified. One is represented by small bright particles protruding above the alumina layer (Fig. 1a, ii). They were found to be rich in yttrium and are referred to as reactive element (RE)-rich particles in the following. The second interesting feature (Fig. 1a, iii) was bright domains

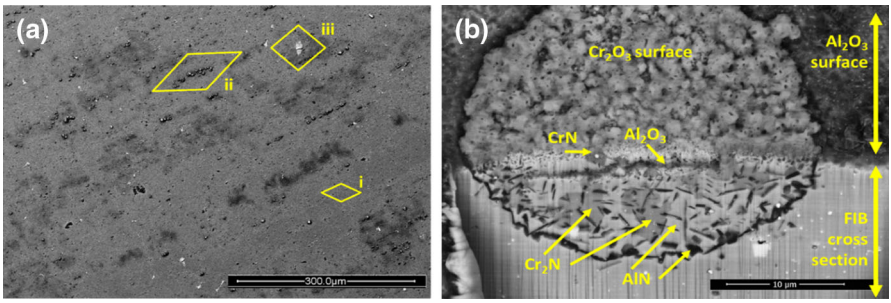

Fig. 1 **a** SEM/BSE image of Kanthal APMT after 168 h in N_2–5%H_2 at 900 °C showing following regions: (*i*) alumina scale; (*ii*) rich in reactive element-containing particles and (*iii*) chromia-containing (*bright* in the image); **b** a FIB cross section through a Cr_2O_3-containing domain at 45° tilt angle. A chromia layer (*bright* in (**a**)) is situated on *top* of an Al_2O_3 layer with *darker contrast*. The alloy matrix beneath the Cr_2O_3 domain is nitrided, consisting of a mixture of needle-shaped AlN particles, Cr_2N and CrN particles and Fe metal. The nitrided volume is separated from the rest of the alloy by a continuous AlN rim

which were rich in chromium, being slightly higher than the surrounding alumina layer. After exposure, the continuous alumina layer had an average thickness of ~2 µm. Cross sections revealed no nitridation of the alloy beneath the undisturbed alumina layer. Also, nitridation was absent below the RE particles. The cross section in Fig. 1b was prepared by eroding through the centre of a chromia domain using FIB. It is typical of several chromia domains on different samples that were cross sectioned in the same way. The circular chromia domain covers a roughly hemispheric region in the alloy substrate which contains a variety of precipitates. The original alumina scale can be seen underneath the chromia layer. The heavily corroded 'pocket', which had a diameter of about 30 µm, is separated from the less-corroded alloy by a seemingly continuous layer of needle-shaped particles. Analysis by TEM/EDS revealed that this layer consisted of AlN. Also, TEM/EDS analysis of the corroded region revealed that it consisted of a dispersion of needle-shaped AlN particles and larger, more equiaxed Cr_2N particles in an iron matrix. In addition, CrN particles were found, both in the nitrided volume and in the chromia layer. Nitride precipitates were not observed beyond the hemisphere, implying that the AlN layer is an effective barrier to nitrogen transport into the alloy. In many cases, the aluminium nitride rim had developed preferentially along alloy grain boundaries, causing the nitrided volume to be less symmetric than that shown in Fig. 1b. However, the composition, shape and distribution of nitride particles were similar, irrespective of whether nitridation was symmetrical or not. In a few cases, the aluminium nitride rim did not close and nitrogen entered into the alloy rather uniformly. In those cases, chromium nitride precipitates were few and only appeared close to the surface. This is interpreted in terms of a lower activity of nitrogen in the remaining alloy which appears because of the continuing consumption of nitrogen by AlN formation in the alloy interior.

Nitridation Sequence

The results indicate that, once the nitrogen accesses to the alloy is established across the scale, the alloy in the vicinity of the point-of-entry quickly reacts with nitrogen. The drive to incorporate nitrogen in the alloy is owing to formation of the highly stable aluminium nitride, AlN, which forms in the corroded alloy matrix, see Fig. 1b:

$$1/2N_2 \rightarrow N(\text{alloy}) \text{ followed by } N(\text{alloy}) + Al(\text{alloy}) \rightarrow AlN(s).$$

The hemispheric shape of the nitrided volume is attributed to the point-of-entry of nitrogen into the alloy being a single location at the scale/alloy interface, in the centre of the chromia domain. In this scenario, during the early stages of nitridation, the rate of N diffusion into the alloy is high compared to the rate of Al diffusion in the opposite direction (D_N in FCC $\sim 10^{-7}$ cm^2/s (900 °C); D_{Al} in FeCrAl (BCC) $\sim 10^{-10}$ cm^2/s (1000 °C) [6, 16]), resulting in the formation of AlN precipitates in the alloy matrix. The radial growth of the internally nitrided 'pocket' causes the nitrogen concentration gradient in the remaining alloy to decrease, resulting in slower transport of N into the alloy. It is suggested that the formation of a continuous AlN layer at the periphery of the nitrided 'pocket' corresponds to a critical radius where the conditions for the formation of a continuous scale are fulfilled, meaning that the flux of nitrogen into the alloy is slower than the outward flux of aluminium. Thus, $N_N D_N \ll N_{Al} D_{Al}$ (N_N = mole fraction of N in the alloy; D_N = diffusivity of N in the alloy; N_{Al} = mole fraction of Al in the alloy; D_{Al} = diffusivity of Al in the alloy). The depth of nitridation in Fig. 1b is about 10 μm. Different radiuses were observed. As noted above, the results imply that the continuous AlN layer formed around the nitrided alloy 'pockets' stops further nitrogen ingress into the alloy. This is expected to cause the concentration of dissolved N in the nitrided 'pocket' to increase. The nitridation of the alloy in the 'pocket' is illustrated by the calculated Fe–23 wt% Cr/N phase diagram in Fig. 2, considering that all aluminium has been consumed. The observation of dichromium nitride (Cr_2N) and chromium nitride (CrN) in the nitrided volume (see Fig. 1b) is in accordance with the phase diagram. The presence of CrN, which is only marginally stable in 95%N_2 at 900 °C (see Fig. 2a), implies that the remaining metal is close to saturation with respect to nitrogen. The large size of the dichromium nitride particles as compared to AlN suggests higher nitrogen mobility in the hexagonal Cr sublattice by utilizing the partially unoccupied octahedral interstitial sites. Moreover, the lower stability of Cr_2N as compared to AlN (see Fig. 2a) also supports more efficient Ostwald ripening (OR) in case of the former, while apparent longer life times of small AlN grains is observed in line with higher activation energies for OR. With 21 wt% Cr, Kanthal APMT^{TM} is ferritic at the exposure temperature. This is also the case for the corresponding Al-depleted alloy (see Fig. 2a). However, because of the precipitation of chromium nitride, the chromium concentration will drop below 12 wt% which is the border between bcc and fcc at 900 °C. Also, Fig. 2a shows that nitrogen stabilizes the fcc lattice. Upon reaching 1.5 wt% nitrogen in the "corrosion pocket", the remaining matrix converts completely into

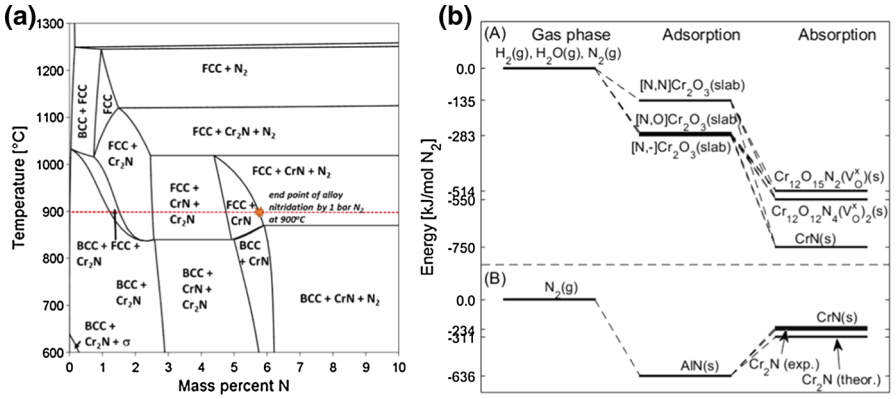

Fig. 2 **a** Fe–23 wt% Cr/N phase diagram (calculated by Thermocalc 5.0, TCFE8 database). The *dotted line* indicates the exposure temperature (900 °C). **b** (*A*) First-principles DFT energy landscape for chromia short-circuiting the Al_2O_3 barrier oxide. N_2 dissociation and N incorporation in the oxide, cf. corresponding structures in *panel right* and text. The short-circuiting oxy-nitrides disproportionate spontaneously to CrN and Cr_2O_3 (see text). (*B*) Net enthalpies of nitridation of aluminium and chromium, once the short-circuiting path is established

fcc structure. Figure 2a implies that the thermodynamic end point of the nitridation of alloy APMT^{TM} by 1 atm N_2 at 900 °C is a mixture of AlN, CrN and fcc iron saturated with N.

Working Hypothesis

The observed microstructure of nitridation strongly suggests that nitrogen enters the alloy via the Cr_2O_3 domains. Thus, the Cr_2O_3 domains appear to cause the Al_2O_3 scale to be short-circuited with respect to nitrogen. The absence of evidence for cracks and pores through the scale suggests that Cr_2O_3 has a key role in the transport of nitrogen across the scale. Such transport may occur by diffusion of nitrogen species at interfaces between Cr_2O_3 and Al_2O_3 but also by transport through Cr_2O_3 grain boundaries or through the Cr_2O_3 particles. As it turns out, testing the validity of the latter case by means of 1st principle calculations becomes straightforward. Indeed, checking the internal consistency of the emerging understanding also becomes relatively easy for transport through Cr_2O_3. The proposed working hypothesis includes dissociation of N_2 at coordinatively unsaturated metal sites (CUS) made possible by the low oxygen activity conditions (compare "Computational Methods" section). The low oxygen activity is of dual origin, i.e. H_2(g) at the gas/oxide interface and the reducing metal/oxide interface, both offering sinks for oxygen and nitrogen. Any diffusion of nitrogen through the Cr_2O_3 bulk would imply intermediate incorporation of nitrogen in Cr_2O_3. The drives for this particular process would be threefold, deriving from (a) the high stability of Al_2O_3 (ΔH_f: −1675 kJ/mol) as compared to Cr_2O_3 (ΔH_f: −1134 kJ/mol) acting to reduce chromium oxide at the oxide/metal interface, (b) the re-oxidation of the oxygen deficient chromium oxide by H_2O as well as by N_2 and (c) the significant drive for internal nitridation whereby AlN is formed (ΔH_f(AlN): −318 kJ/mol). The stability

of AlN can be compared to, e.g. chromium nitride (ΔH_f(CrN): −117 kJ/mol and (ΔH_f(Cr_2N): −125 kJ/mol). Actually, the last step, i.e. the internal nitridation of aluminium, disallows the build-up of a chromium oxy-nitride barrier for as long as unreacted Al is present in the matrix. However, a necessary condition for this scenario, i.e. bulk diffusion of nitrogen through the Cr_2O_3 particle, requires metastable chromium oxy-nitride intermediates as represented by reactions of the formula:

$$Cr_2O_3(s) + \frac{y}{2}N_2(g) + yAl(s) \rightarrow Cr_2N_yO_{3-\frac{3y}{2}}(V_O^{**})_{\frac{y}{2}}(s) + \frac{y}{2}Al_2O_3(s).$$

The formula captures the fact that Cr_2O_3 interacts with two media, one being N_2(g) and the other aluminium in the alloy. The products are Al_2O_3 and a defect-rich transient chromium oxy-nitride compound. The latter compound was not detected experimentally. Yet, the viability of any such metastable oxy-nitride moiety would suggest it to be representative of a set of oxy-nitride compositions, lending support to the existence of a corresponding route for nitrogen to penetrate the oxide scale.

Validation of the Working Hypothesis by Means of First Principle Models

Two sets of calculations were performed to explore this hypothesis. One set addresses the incorporation of nitrogen into the oxide lattice, while the second set tests the possible validity of metastable oxy-nitrides implied by effective inwards transport of nitride ions. The former employs "slab" calculations that are utilized to model processes occurring on surfaces and, to some extent, at grain boundaries. The oxy-nitride calculations address transformations in the bulk. In the first set of calculations, the ability of Al_2O_3 and Cr_2O_3 layers to bind nitrogen was tested. Metal nitrides were employed as nitrogen sources to test the "stickiness" (ability to chemisorb) of N onto the reduced Al_2O_3 and Cr_2O_3 surfaces.

Employing the notation $[-,-]$ to denote two coordinatively unsaturated surface sites (CUS) in accord with Eqs. 4–6, we consider first $[-;A] \equiv [-,-]$ and $[N;A] \equiv [N,-]$ to obtain $\Delta\tilde{H}_{Al}^{N;-} = -28.1$ kJ/mol and $\Delta\tilde{H}_{Cr}^{N;-} = -141$ kJ/mol. It becomes interesting to estimate the corresponding Gibbs energies. In as much as the entropy contribution for N_2 is of the order of 60 kJ/mol already at room temperature, this renders N_2 dissociation at Al^{3+} CUS sites on Al_2O_3 non-spontaneous by $\sim$180 kJ/mol N_2 at 900 °C. This is in contrast to the Cr_2O_3 surface, which displays a sufficiently high exothermic adsorption enthalpy at Cr^{3+} CUS sites, i.e. −282 kJ/mol, to render the dissociation exergonic at 900 °C by approximately −40 kJ/mol N_2 when taking the entropy contribution into account.

In order to test the sensitivity of surface nitridation to surface termination, 50% oxygen coverage of the CUS sites was also considered, that is (cf. Eqs. 4–6 again) $[-;A] \equiv [-,O]$ and $[N;A] \equiv [N,O]$. In case of Cr_2O_3, $\Delta\tilde{H}_{Cr}^{N;O} = -135$ kJ/mol was obtained implying that partial pre-oxidation of the Cr_2O_3 slab results in approximately unchanged reactivity of the remaining CUS. In the case of Al_2O_3, an endothermicity of $\Delta\tilde{H}_{Al}^{N;O} = +39.1$ kJ/mol was obtained. In this case, NO formation

occurs rather than N and O occupying one CUS each, pointing towards an inability to co-chemisorb nitrogen and oxygen to the Al_2O_3 surface under investigation.

In addition, we may address the case of 100% nitrogen coverage on CUS. In accord with Eqs. 7–9, $\Delta\tilde{H}^{N;N}_{Al} = -93.9$ kJ/mol; $\Delta\tilde{H}^{N;N}_{Cr} = 135$ kJ/mol are obtained. In the case of Al_2O_3 however, the stability is owing to residual N–N bonding. This is in contrast to Cr_2O_3 where the nitrogen molecule has undergone complete dissociation resulting in two chemisorbed N, each occupying a CUS. It is noted here that there is a coverage dependence in the chemisorption energy of N to Cr_2O_3 in that 100% coverage displays half the exothermicity of that of 50% coverage. For the nitridation process, this implies an N_2 dissociation-related bottleneck owing to the entropy contribution to Gibbs energy, i.e. the reaction Gibbs energy to form the [N,N] intermediate on Cr_2O_3 becomes endergonic by 105 kJ/mol at 900 °C. For comparison, −40 kJ/mol reaction Gibbs energy was estimated above for the formation of 2[N, −] at said temperature (see above). The absence of catalytic sites for N_2 dissociation on the Al_2O_3 scale would render the surface nitridation of Al_2O_3 inaccessible. Indeed, the overwhelming preference for nitrogen chemisorption to Cr_2O_3 implies that it acts as an efficient sink towards any Al_2O_3-associated nitrogen. After establishing the drive to chemisorb nitrogen onto chromium oxide, a small yet significant enhancement in stability was found for nitrogen incorporation subsurface in the Cr_2O_3 scale (to be published). Here, it becomes important to identify possible routes for nitrogen diffusion through the Cr_2O_3 bulk as driven by the internal nitridation of aluminium in the alloy, acting as a sink towards nitrogen from the atmosphere. This is done here by searching for possible candidate transient species among chromium oxy-nitrides, being constrained to preserve the +III oxidation state of the chromium ions. This constraint implies the replacement of two O^{2-} ions by two N^{3-} ions to require the removal of a third O^{2-} ion, i.e. the introduction of an oxygen ion vacancy. The possible existence of such a compound under quasi-steady state conditions during nitridation is based on reaction enthalpy arguments. Consider the reaction

$$Cr_{12}O_{18}(s) + 2AlN(s) \rightarrow Cr_{12}N_2O_{15}(V_O^{**})(s) + Al_2O_3(s) \quad (10)$$

for which we get +123 kJ/mol endothermicity. Shifting the reaction energy by the $2 \times (-318)$ kJ/mol enthalpy of the formation of 2AlN(s), we obtain −514 kJ/mol for the reaction:

$$Cr_{12}O_{18}(s) + N_2(g) + 2Al(s) \rightarrow Cr_{12}N_2O_{15}(V_O^{**})(s) + Al_2O_3(s). \quad (11)$$

A plateau in the stability of chromium oxy-nitrides is indicated from the fact that ~570 kJ/mol exothermicity is obtained for the further Al_2O_3-driven nitridation:

$$Cr_{12}N_2O_{15}(V_O^{**})(s) + N_2(g) + 2Al(s) \rightarrow Cr_{12}N_4O_{12}(V_O^{**})_2(s) + Al_2O_3(s). \quad (12)$$

A limiting case is offered by the reaction

$$N_2(g) + Cr_2O_3 + 2Al(s) \rightarrow 2CrN + Al_2O_3 \quad (13)$$

which is exothermic by $\sim$750 kJ/mol, emphasizing the transient nature of the chromium oxy-nitride. Along this line, DFT also gets the disproportionation reaction

$$Cr_{12}O_{15}N_2(s) \rightarrow 5\ Cr_2O_3(s) + 2\ CrN(s) \quad (14)$$

to be exothermic by $\sim$200 kJ/mol. Consequently, the lack of evidence for chromium oxy-nitride is not surprising. Rather, it becomes tempting to ascribe any emergence of apparently isolated grains of CrN in the Cr_2O_3 layer (see Fig. 1b) to such a disproportionation reaction, competing with the short-circuiting mechanism for internal nitridation at longer exposure times. Thus, support from DFT for a sufficient bulk transport channel for internal nitridation emerges (a) dissociation of N_2 on Cr^{3+} CUS sites on the chromia surface and (b) subsequent inward diffusion of nitrogen in the form of nitride ions through a chromia layer being facilitated by the co-existence of oxygen vacancies.

The Role of Aluminium in Nitridation

In a dry N_2–5%H_2 environment, aluminium takes a dual role in the corrosion of FeCrAl: (1) The most pronounced aspect is the resilience of the protective Al_2O_3 scale. Covering 99% of the surface area, it offers protection against the thermodynamic drive for alloy nitridation. Thus, cross sectioning showed no nitridation whatsoever of the alloy substrate below the intact Al_2O_3 scale. (2) Because of the high stability of Al_2O_3, less stable oxides in the scale, including Cr_2O_3, can be reduced by aluminium in the alloy. This offers a means to short-circuit the scale towards alloy nitridation. As shown in Fig. 1a, local Cr_2O_3 enrichments are embedded in the Al_2O_3 scale. These Cr_2O_3 domains are subject to low oxygen activity due to the dual influence of H_2 in the atmosphere and the aluminium-rich alloy at the bottom of the scale. At the latter interface Cr_2O_3 in fact reaches its dissociation pressure, Cr_2O_3 being stable at oxygen activities $>10^{-25}$ at 900 °C, while Al_2O_3 formation is spontaneous at oxygen activities $>10^{-39}$. Consistency of these findings is provided by DFT calculations, which demonstrate the powerful drive to oxidize aluminium while causing the formation of chromium oxy-nitrides. This implies that the presence of a chromia domain penetrating the alumina scale will allow transport of nitrogen across the scale, short-circuiting the protective Al_2O_3 layer. At steady state, besides Al consuming oxygen from the chromium oxy-nitride transient, the internal nitridation of Al is also accessed. The consumption of aluminium in the alloy by internal nitridation of Al and the subsequent formation of internal chromium nitrides cause swelling of the alloy. Also, it may be noted that the resulting mixture of fcc iron, CrN and AlN in the nitrided alloy is likely unable to form a protective scale when exposed to high oxygen activity environments at high temperature. Work on the nature of the initial defects in the Al_2O_3 scale which render the resulting scale non-protective by the corrosion process described is in progress.

Conclusions

The corrosion of the FeCrAl alloy APMT^{TM} in a dry N_2–5%H_2 environment at 900 °C was studied. Corrosion manifested itself as nitrided 'pockets' in the alloy below chromia domains in an otherwise protective Al_2O_3 scale. The nitrided regions consisted of a dispersion of needle-shaped AlN particles and larger, more equiaxed Cr_2N particles in an iron matrix and were separated from the uncorroded alloy by a continuous AlN layer. CrN particles were associated to Cr_2O_3. This behaviour was interpreted in terms of local short-circuiting of nitrogen transport across the scale by chromia and subsequent alloy nitridation. 1st principles calculations were used to investigate the role of chromia for nitrogen transport. The calculations showed that the adsorption of nitrogen via CUS at a chromia surface is favoured, while the corresponding process on Al_2O_3 is not viable. Also, 1st principles calculations showed that the formation of metastable chromium oxy-nitride compounds by the reaction of aluminium, N_2 and chromia is spontaneous. Thus, it is proposed that the nitridation of the FeCrAl matrix by nitrogen occurs by (a) dissociation of molecular nitrogen on Cr^{3+} CUS sites on the chromia surface and (b) subsequent inward diffusion of nitrogen in the form of nitride ions through a chromia layer.

References

1. J. Young, in *Corrosion Series*, ed. Y. D. John (Elsevier Science, Amsterdam, 2008), p. 315.
2. A. H. Heuer, *Journal of the European Ceramic Society* **28**, 1495 (2008).
3. B. A. Pint, in *Shreir's Corrosion*, ed. J. A. R. Tony (Elsevier, Oxford, 2010), p. 606.
4. R. Orosz, U. Krupp, and H.-J. Christ, *Zeitschrift für Metallkunde* **96**, 775 (2005).
5. H. J. Christ, S. Y. Chang, and U. Krupp, *Materials and Corrosion* **54**, 887 (2003).
6. G. Y. Lai, *High-Temperature Corrosion and Materials Applications*, (ASM International, Materials Park, 2007).
7. B. S. Jönsson and C. Svedberg, *Materials Science Forum* **251–254**, 551 (1997).
8. F. Liu, et al., *Oxidation of Metals* **83**, 441 (2015).
9. V. Kochubey, et al., *Materials Letters* **60**, 1654 (2006).
10. B. Jönsson, et al., *Oxidation of Metals* **79**, 29 (2013).
11. G. J. Tatlock, et al., *Materials and Corrosion* **56**, 867 (2005).
12. M. D. Segall, et al., *Journal of Physics* **14**, 2717 (2002).
13. *Materials Studio* 6.0. *Accelry Inc.,* (*Simulation Software*).
14. H. J. Monkhorst and J. D. Pack, *Physical Review B* **13**, 5188 (1976).
15. *Data from NIST Standard Reference Database* 69. NIST Chemistry Webbook (2016).
16. L. Maréchal, et al., *Oxidation of Metals* **60**, 1 (2003).